# Molecular Dynamics Simulations of Particle Bombardment Induced Desorption Processes: Alkanethiolates on Au(111)

**K. S. S. Liu,[†] C. W. Yong,[‡] B. J. Garrison,[§] and J. C. Vickerman*,[†]**

*Surface Analysis Research Centre, Department of Chemistry, UMIST, PO Box 88, Manchester, M60 1QD, U.K., School of Biological Sciences, University of Manchester, Stopford Building, Oxford Road, Manchester, M13 9PT, U.K., and Department of Chemistry, The Pennsylvania State University, University Park, Pennsylvania 16802*

*Received: October 14, 1998; In Final Form: January 28, 1999*

Molecular dynamics has been used to model Ar atom induced sputtering of *n*-alkanethiolate molecules self-assembled on Au(111). The aim is to discover possible mechanisms of formation of the various sputtered species such that their relationship to surface chemistry can be understood. To model the system, a blend of pairwise and many-body potentials are used to represent the interatomic interactions. To simulate the formation of gold−thiolate clusters required the development of the potential for the Au−S interaction. The resulting model predicted a "mass spectrum" of atomic and cluster species which is remarkably similar to the experimental static SIMS spectra of *n*-alkanethiolate SAMs on gold. A number of emission mechanisms for the production of hydrocarbon fragments and gold−thiolate clusters are suggested by the model which provide very valuable insights into the relationship between the spectral features and surface chemistry.

## Introduction

Static secondary ion mass spectrometry (SSIMS) has been shown to be a powerful technique for surface chemical analysis of complex organic and bioorganic materials.[1] The mass spectra usually contain ions (quasi-molecular ions and fragments) which can be directly related to the molecular structure of the molecules of interest using interpretational approaches not dissimilar to those used in conventional mass spectrometry. Usually there are also a number of other ions that originate from the bonding of the organic system to a metal substrate support, or from combinations of fragment ions and molecular species. Our understanding and interpretation of these more complex peaks in the SSIMS spectra is inhibited by the lack of a satisfactory model for the mechanism of sputtering of organic layers.

Molecular dynamics simulations have been very successful in providing a detailed understanding of the mechanism of sputtering of metal surfaces.[2−12] These simulations demonstrate the importance of interatomic collisions within the solid, initiated by the primary particle impact, in generating the emission of detectable (i.e., relatively low kinetic energy) atomic and cluster species remote from the point of impact. More recently, the approach has been extended to studies of the sputtering of simple organic layers adsorbed on metal surfaces.[13−20] Here it was shown that in addition to sputtering of organic species due to metal atoms emerging from below, organic fragments sputtered from the layer could collide with other adsorbed molecules to provide another significant emission pathway.[16−20] In order to extend the model to longer chain length organic systems, this study applies the molecular dynamics approach to the sputtering of *n*-alkanthiolate molecules self-assembled on Au(111).

The fact that the adsorption of *n*-alkanethiolate molecules on a Au(111) surface results in highly organized self- assembled monolayers (SAMs) has been known for many years.[21] Their relative ease of preparation and the fact that their surface structure has been extensively characterized make them an ideal system to use as a model to investigate the mechanism of sputtering of organic layers supported on a metal substrate. The densely packed layers of $S-(CH_2)_n-CH_3$ bonded to the gold surface through the S atom at an angle of approximately 30° to the surface normal provides a system in which the influence of adsorbate bonding at the surface and of carbon chain length on the mechanism of sputtering can be investigated.[22−25]

StaticSIMS has been exploited in probing the surface chemistry of SAMs.[26] The experimental mass spectra seem to reflect the chemical state of the substrate−adsorbate interface.[27−33] The positive and negative secondary ion spectra, however, are rather different. The positive ion yield is relatively simple and is dominated by a Au ion signal. The main cluster ions are one and two gold atoms associated with a thiolate molecule and $Au(CH_2)_n$ ions. The negative ion spectrum is extremely rich in high-intensity ions, particularly gold and thiolate species combined in various relative numbers. There are also ions formed from combinations of gold and sulfur. In both spectral series there are ions formed by fragmentation of the parent thiolate. At first sight the pattern of ejected species is not easily related to the surface structure of the system, however, the yield of the cluster ions (e.g. AuM, where M is the thiolate species) has been shown to be directly related to surface coverage of the thiolate.[34] This opens up the possibility of SSIMS being used as a tool to investigate the surface order for a variety of assemblies. Indeed, studies have shown that SSIMS is able to probe the structure and composition of mixed monolayers formed from mixtures of alkanethiolates.[28,34−37] SSIMS spectra are observed which are consistent with the ejection of Au dialkanethiolates molecules, $AuM_2$ $AuM'_2$ and AuMM′, where M and M′ are the parent alkanethiolates present on the surface.

* To whom correspondence should be addressed.
[†] UMIST.
[‡] University of Manchester.
[§] The Pennsylvania State University.

10.1021/jp984071k CCC: $18.00 
Published on Web 04/01/1999

It seems that these sputtered species may be used for the elucidation of the lateral distribution of molecules for mixed overlayers.[28,34,37]

The spectral data highlight the need for an adequate model of the sputtering and the secondary ion formation processes from organic layers. At present it is not possible to tackle the ionization problem, but our molecular dynamics approach should enable us to investigate the mechanism of sputtering. A number of questions arise from the data. Can all the sputtered species arise solely from the deposition of primary ion energy into the gold substrate and the subsequent upward movement of gold atoms against the adsorbed molecules? The data suggests that other pathways to particle emission are also involved. Apart from the obvious possibility that excited emitted species can fragment due to unimolecular decomposition during the flight to the detector, is it possible that gold atoms or other emitted fragments can collide with adsorbed species and form either new fragments or new adduct species? Is it possible that as the primary ion passes through the organic layer some energy is lost resulting in emission from the organic layer? How are the cluster species that involve complete alkanethiolate molecules formed? For example, is the Au dialkanethiolate created from the ejection process where neighboring molecules participate in the cluster, or are they formed as the species emerge in the surface region?

We have reported earlier on a number of exploratory MD simulation studies of the bombardment process on an *n*-alkanethiolate system supported on a Au substrate.[38,39] In these studies we have shown that that the MD formalism was required to be modified in order to account for the change in Au−S bond strength as the configuration changes from having the thiolate on the surface to having a gas-phase species such as $AuM_2$ . It was shown that when a modified Morse potential for the Au−S interactions is used in the simulation model, a significant yield of gold-thiolate clusters was obtained. Most of these clusters were identified and are found to be similar to those recorded experimentally.[27−30] In this report, we describe the modified Au−S potential. In addition, we report the full mass spectrum of species that eject. On the basis of the model, probable mechanisms for the formation of various ejected species including hydrocarbon fragments and gold−thiolate clusters which occur in the early stages of bombardment events are suggested. Even though the calculations cannot quantitatively predict decomposition of the larger sputtered molecules during the several 10s of microseconds flight to the detector, nor even qualitatively describe ionization, we have been able to use the results from the simulations to explain almost all of the major peaks in the experimental mass spectra.

## Method

The Ar bombardment process of alkanethiolate molecules, $S-(CH_2)_4-CH_3$, adsorbed on a Au(111) surface is studied using molecular dynamics (MD) computer simulations. The MD scheme has been described in extensive detail elsewhere.[5,40−43] Briefly, it consists of integrating Hamilton's equations of motion over some time interval to determine the position and velocity of each particle as a function of time. The energy and forces in the system are described by many-body interaction potentials. Experimentally observable properties, such as total yield, mass spectrum, kinetic energy, and angular distributions are calculated from the final positions, velocities, and masses of all the ejected species. Mechanistic information is obtained by monitoring the time evolution of important collisional events.

The model consists of approximating the Au(111) substrate by a finite microcrystallite containing 2592 Au atoms arranged in 9 layers of 288 atoms each. A total of 68 alkanethiolate molecules are placed on the 3-fold sites of the Au surface in a $(\sqrt{3}\times\sqrt{3})R30°$ arrangement as shown in Figure 1. The entire system is quenched to a minimum energy configuration prior to Ar atom impact. An Ar atom with 700 eV of kinetic energy is directed at an angle parallel to the direction of the tilt of chains. A total of 2100 Ar aiming points or trajectories directed within the impact area of a parallelogram (shown as shaded area in Figure 1) are calculated. This impact area encompasses all the possible unique aiming points on the surface. Each trajectory is initiated using a fresh undamaged sample. The trajectory is terminated when the total energy of any atom remaining in the solid is so low that ejection becomes improbable. The termination time ranges up to 2 ps and depends on the impact point of the primary particle and the manner in which the energy distributes within the solid. Open boundary conditions are used for the system.[41,43] That is, energetic particles that reach the sides or bottom of the computational cell are allowed to exit, taking their energy with them. In the real system, these energetic particles would transport energy into the regions of the solid further from the impact zone and not influence the ejection process.

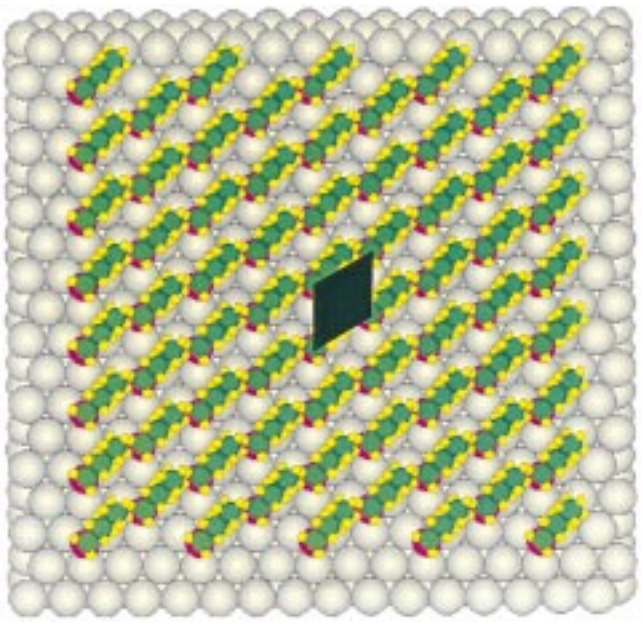

**Figure 1.** Top of the system of 68 *n*-alkanethiolate chains adsorbed on a Au(111) surface. The parallelogram outlined represents the impact area in which the Ar atom is directed. The angle of incidence is parallel to the chains or approximately from the upper right corner in the figure. The gray, red, green, and yellow spheres represent Au, S, C, and H atoms, respectively. There is also a gradation of sizes which will be used in subsequent figures even though the colors change.

A blend of empirical pairwise and many-body potential energy functions is used to represent the forces among the various atoms. We will first describe the interactions that have been used previously by others and then discuss the potential that we are introducing here.

We use a purely repulsive Molière potential[44] to describe all interactions between the Ar and other atoms. This assumption is based on the fact that the Ar atom primarily imparts energy and momentum to the system and does not play a direct role in the chemistry of the bombardment process.

For the remainder of the system, both the repulsive and attractive interactions are evaluated using many-body and pairwise potential functions. The Au−Au interactions are described by the molecular dynamics/Monte Carlo corrected effective

**TABLE 1: Parameters Used in the Pairwise Potentials**

| interactions | potential type | $\epsilon$/eV | $D_e$/eV | $R_e$/Å | $\alpha$/Å$^{-1}$ |
|---|---|---|---|---|---|
| S−S | Morse | | 0.15−2.757[a] | 2.019[b] | 1.72 |
| S−C | Morse | | 2.684[a] | 1.808[c] | 1.867 |
| S−H | Lennard-Jones | 0.40 | | 1.80 | |
| Au−S | Morse | | 0.365−2.59 | 2.70 | 1.47 |
| Au−C | Lennard-Jones | 0.00277[d] | | 3.561[d] | |
| Au−H | Lennard-Jones | 0.00179[d] | | 3.083[d] | |

[a] Atkins, P. W. *Physical Chemistry*, 3rd ed.; Oxford University Press: Oxford, U.K., 1986; p 822. [b]Chen, K.; Allinger, N. L. *J. Phys. Org. Chem.* **1991**, *4*, 659. [c] Allinger, N. L.; Quinn, M.; Rahman, M.; Chen. K. *J. Phys. Org. Chem.* **1991**, *4*, 647. [d] Rappe, A. K.; Casewit, C. J.; Colewell, K. S.; Goddard III, W. A.; Skiff, W. M. *J. Am. Chem. Soc.* **1992**, *114*, 10024

medium (MD/MC-CEM) potential function for fcc metals.[45−47] One attractive feature of the MD/MC-CEM potential is that it shows reasonable Coulombic behavior at small internuclear separations, an important aspect in the modeling of a high-energy bombardment process. Rosencrance et al.[8] have used the potential to calculate the energy and angular distributions of ion bombarded Rh and Ni metal surfaces, and successfully reproduced features observed in experimental data. More recently, Chatterjee et al.[48] have applied the potential to model a Ag surface with a benzene overlayer to study the keV particle bombardment process. The calculated energy and angular distributions of $C_6H_6$ match well with the experimentally measured distributions. Finally, the MD/MC-CEM potential has been used to model thermal properties of alkanethiolate overlayers on Au metal surfaces.[49−51]

The hydrocarbon interactions are described by the Brenner hydrocarbon potential function.[52,53] This potential has been fitted to the energetics and structures of small hydrocarbon molecules including radicals as well as graphite and diamond lattices. It allows for chemical reaction and accompanying changes in atomic hybridization during the course of a reaction. A variety of chemical reactions[54−60] have been successfully modeled by MD simulations using this potential including the compression of buckministerfullerenes between graphite planes,[53] atomic-scale friction,[54] compression-induced structural transition[56] in self-assembled monolayers of alkanethiols on gold, and hydrogen abstraction from hydrogen-terminated diamond surfaces.[57] The potential has also been used in the particle bombardment studies where chemical reactions are modeled among adsorbed molecules supported on a metal. [16−20,38,39,48,61−63] Of note is that this hydrocarbon potential is confined only to short-range interactions of nearest neighbors. Any long-range van der Waals type interactions are not included. This restriction, however, should not cause a problem in our study since this potential is not being used to predict the packing density of the adsorbed overlayer. As described in ref 16, a Molière function is attached to the repulsive wall of the Brenner potential in order to accommodate high-energy collisions.

The interactions for S−C, Au−C, Au−H, S−H, Au−S, and S−S are described by pairwise potential functions and their parameter values are listed in Table 1. In general, Morse potentials are used for bonding interactions and Lennard-Jones potentials for van der Waals interactions. The basic S−C interaction is a Morse potential.[64] Since the S atom is attached to a C atom in the chain, the carbon atom must account for the S neighbor in order to have the correct geometry. In order to achieve this, the S atoms are treated as if they were H atoms in the Brenner potential and the S−C bonds are assumed to have $\sigma$-type character. In much the same way, the Au−C interactions are described with a Lennard-Jones pairwise potential, which is also blended into Brenner's hydrocarbon potential. This approach is similar to that adopted by Taylor et al. for the Pt−C interactions in the hydrocarbon/Pt systems[16] and details on the merging of potentials can be found therein. The nonbonding type of interactions for Au−H and S−H are also modeled by a Lennard-Jones potential defined with an energy parameter, $\epsilon$, and an equilibrium distance, $r_e$.[65] Note that the values for S−H interactions are chosen primarily to maintain the tetrahedral structure of the C atom attaching directly to the S atom of the chain. In addition, we found that if the parameters for a bonding potential (i.e., large $\epsilon$) are used, the hydrogen atoms of this carbon would unrealistically attach to the S atom due to strong interaction between S and H atoms. Conversely, nonbonding parameter sets (i.e., large $r_e$) would cause the hydrogen atoms to repel from the S and break the C−H bond. Hence, the parameters shown in Table 1 have been used in order to compromise between the two extreme conditions.

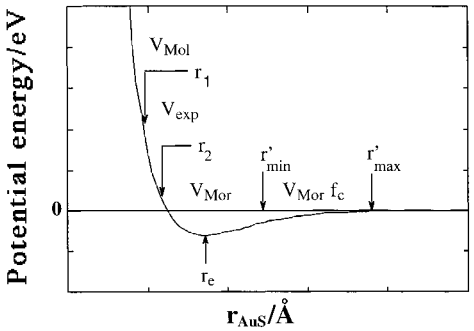


**Figure 2.** Graphical representation of the modified Au−S potential with $D_e = 1.2$ eV. The diagram shows the positions at which the various functions exist. $V_{Mol}$ is the Moliére potential, $V_{exp}$ is the exponential function, $V_{Mor}$ is the Morse potential, and $V_{Mor}f_c$ is the Morse potential splined to a cutoff function $f_c$. $r_e$ is the equilibrium distance. (See text for more detail.)

A modified Morse potential has been applied to Au−S interactions because we are interested in modeling the Au−thiolate clusters.[38,39] The potential has a variable energy parameter of the Morse potential well depth, $D_e$, which varies according to the height of the Au and/or S atoms above the surface. The reason for such a modification is that the appropriate value of $D_e$ of 0.365 eV for the Au−S interaction on the surface[49,50] is too small to describe the bonding character of a molecular gold-thiolate in the gas phase. In order to account for this behavior, a simple approach is devised based on the modification of a conventional Morse potential by varying $D_e$ as a function of the perpendicular distance, $\mathbf{r}_y^{\perp}$, of an Au−S pair from the surface. The modified potential is made up of several functions blended together as shown in Figure 2, and has the formula,

$$V_{mor}(\mathbf{r}_{AuS}, D_e(\mathbf{r}_y^{\perp})) = D_e(\mathbf{r}_y^{\perp}) f_c(\mathbf{r}_{AuS}, r'_{max}(\mathbf{r}_y^{\perp})) \times \{e^{2\alpha(r_e-\mathbf{r}_{AuS})} - 2e^{\alpha(r_e-\mathbf{r}_{AuS})}\} \quad (1)$$

where $\alpha$ is the range and $r_e$ is the equilibrium distance for the Au−S bond. The well depth $D_e$ is a function of the vertical height above the surface

$$D_e(\mathbf{r}_y^{\perp}) = \gamma + \beta \cos\left[\frac{\pi(\mathbf{r}_y^{\perp} - r_{max})}{(r_{min} - r_{max})}\right] \quad (2)$$

where $r_{min} \le \mathbf{r}_y^{\perp} \le r_{max}$. The values of $\gamma$ and $\beta$ are 1.4775 and 1.1125 eV, respectively. These values are determined such that the Au−S pair would have a full adsorbate character with $D_e = 0.365$ eV when the $\mathbf{r}_y^{\perp}$ values of both Au and S are less than

$r_{min}$. Conversely, the Au−S interaction would retain a full gas phase character with $D_e = 2.59$ eV[66] when the $\mathbf{r}_y^{\perp}$ values are greater than $r_{max}$. The values for $r_{min}$ and $r_{max}$ have been taken as 3.0 and 6.5 Å, respectively. The choice of the $D_e$ function (eq 2) allows for a smooth gradual change of $D_e$ as $r_y^{\perp}$ approaches either of the extremes. We have tested the operation of the potential with other values for $r_{min}$ and $r_{max}$ and it was found that if the range chosen is too near to the surface, an unreasonably large yield of gold clusters would result. If the range is set too far from the surface, however, the probability for Au and S to form into gold clusters is greatly reduced.

The modified potential is also splined to a cutoff function at long distances. This limits its operation to only short-range interactions for Au and S atoms. This function has the formula,[16]

$$f_c(\mathbf{r}_{AuS}, r'_{max}(\mathbf{r}_y^{\perp})) = \frac{1}{2} + \frac{1}{2}\cos\left[\frac{\pi(\mathbf{r}_{AuS} - r'_{min})}{r'_{max}(\mathbf{r}_y^{\perp}) - r'_{min}}\right] \quad (3)$$

where $r_{min}$ and $r_{max}$ are the respective minimum and maximum distances that the cutoff function is applied. They are initially set to 2.9 and 6.0 Å, respectively. Beyond $r'_{max}$, the potential smoothly decays to zero. Note that the $r'_{max}(\mathbf{r}_y^{\perp})$ changes from 6.0 to 3.4 Å with respect to $\mathbf{r}_y^{\perp}$ according to eq 4.

$$r'_{max}(r_y^{\perp}) = 4.70 + 1.30\cos\left[\frac{\pi(r_y^{\perp} - r_{min})}{r_{max} - r_{min}}\right] \quad (4)$$

where $r_{min}$ and $r_{max}$ have the same values as those used in eq 2. In other words, the $f_c$ in eq 3 ensures a smooth reduction of the cut off range with $r'_{max}$ changes from 6.0 to 3.4 Å while $D_e$ varies from 0.365 to 2.59 eV. In this way, the full bonding character is confined to short range.

In order to properly describe the repulsive energy at short interatomic separations, the potential is splined to a Molière potential using an exponential form[67]

$$V_{exp}(\mathbf{r}_{AuS}) = -\frac{1}{A}e^{A\mathbf{r}_{AuS}+B} + C \quad (5)$$

where $\mathbf{r}_{AuS}$ lies between a minimum distance, $r_1$, at which a pure Molière potential is used, and a maximum distance, $r_2$, beyond which a pure Morse potential is applied. The values of $r_1$ and $r_2$ are chosen as 0.9 and 1.9 Å respectively (see Figure 2). Sets of *A*, *B*, and *C* values are determined uniquely for each $D_e$ such that the functions and their first derivatives are always continuous. Finally, the S−S interactions are also described by a modified Morse potential, similar to that for the Au−S interactions. The height of S atoms above the surface determines the $D_e$ value of the Morse potential, and hence the strength for the S−S interactions. The range of $D_e$ values used is shown in Table 1.

At the end of each simulation, those atoms which have a velocity directed away from the surface and are at a height of 8 Å above the original film are regarded as ejected. For clusters to be ejected, they are also required to cross over the height of 8 Å above the film and to not have any interaction with the surface. The prescription for identifying clusters has been delineated before.[4,5,68] Briefly, pairs of atoms are checked to see if there is an attractive interaction between them in which case they are considered linked. A network of linked pairs is constructed and the total internal energy of the group is evaluated. If the total internal energy is less than zero, then the group of atoms is considered to be an ejected molecule. This prescription, of course, overestimates the number of bound ejected molecules as some of these moieties have sufficient internal energy to unimolecularly decay during the flight to the detector. We could at this stage go through an analysis as done previously for small metal clusters[68] and continue integrating the equations of motion for this group of atoms to longer times. In this case, however, we do not believe that the empirical potential is sufficiently good for all the possible reaction channels such that this exercise is warranted. For small organic species, previous work[16,48] has shown that a simple estimate can be made to determine how unimolecular decay can affect the number of clusters ejected.

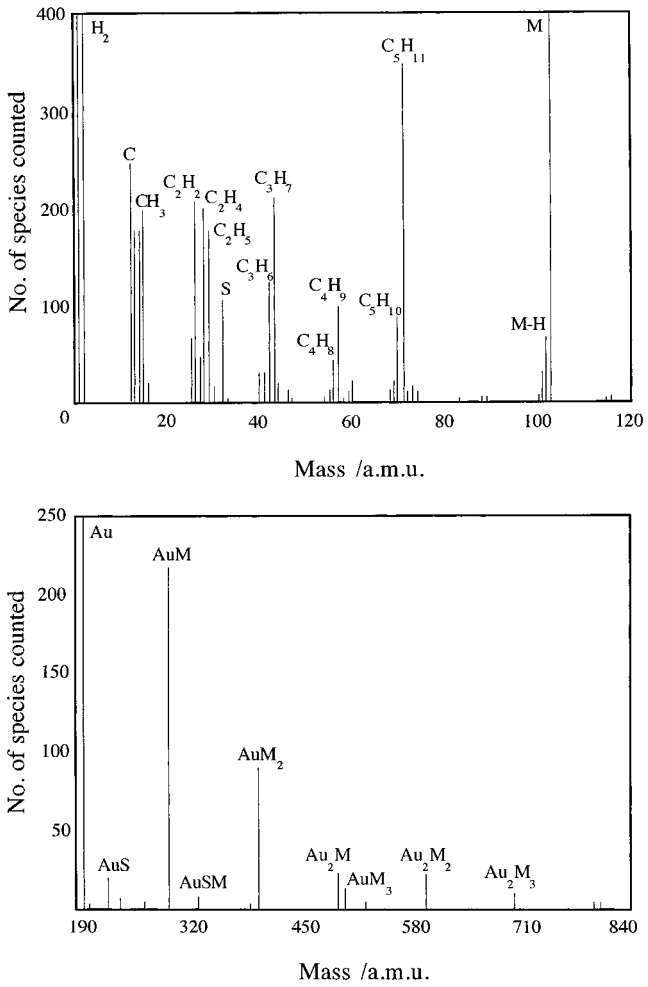


**Figure 3.** Calculated mass spectrum of the alkanethiolate system due to 700 eV Ar bombardment.

## Results

In a typical bombardment process, a high-energy primary atom or molecule is directed onto a system thereby transferring its energy and generating extensive collisions. As a result of these collisions, those atoms and molecular aggregates which have sufficient energy to break away are able to eject to the vacuum. It is these species which reflect the identity and structure of the original system and whose mechanism of emission is therefore of particular interest.

The ejected species are recorded by counting their number according to their masses. For convenience, the calculated mass distributions are plotted as "mass spectra" with the number of species counted (peak intensity) versus cluster mass in atomic mass units (amu) as shown in Figure 3. This graphical representation provides a starting point for identifying major species for further mechanistic analysis. As discussed above,

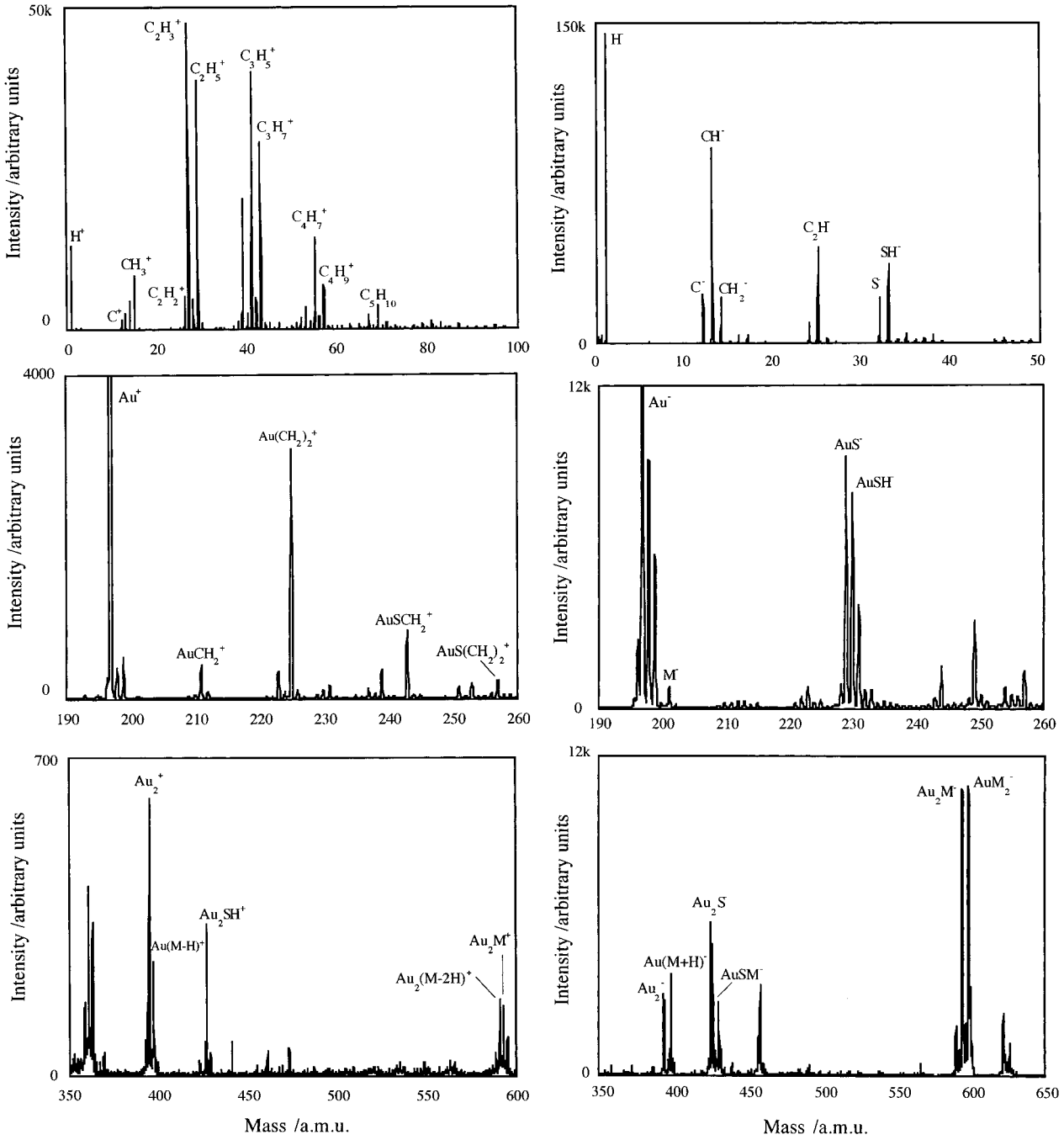


**Figure 4.** Experimental SIMS spectra reproduced from ref 27: (a) positive ions; (b) negative ions. Copyright Surface Spectra Ltd. Reprinted with permission.

the species included in Figure 3 are all the ones that are linked by pairs of atoms that have attractive interactions between them. The mass spectrum is divided into two regions, the low-mass region from 0 to 120 amu which consists mostly of hydrocarbon fragments and the parent molecule, M. The high-mass region is above 190 amu which mainly records ejected species containing Au atoms. There is no significant yield of ejected species in the mass range 120−190 amu. Below we discuss the various peaks in the spectrum and compare them to the experimental spectra, an example of which is reproduced in Figure 4.

In discussing the similarities and differences between the calculated and experimental spectra, it is important to be aware of differences between the two "experiments". For instance, the difference in time scale may affect the overall detection of fragments. Experimentally, the ejected molecules are recorded in a period of 10s of microseconds after the impact. Some of the species ejected from the system may be in excited internal states and are likely to undergo further fragmentation. It is these smaller fragmented species rather than the original ejected molecules which will be recorded by the detector.

As mentioned above, to correct the calculations for stability of the ejected molecules and the decomposition products requires a more sophisticated interaction potential. We do feel, however, that we can estimate how many of the small hydrocarbon species will remain intact.[16,48] To achieve this, the effective internal energy, $E_{\text{eff}}$, is defined for each group of ejected species as a measure of their stability with respect to decomposition. A similar approach and definition for $E_{\text{eff}}$ can be found in eq 4 of ref 16. The probability of decomposition is then estimated by comparing $E_{\text{eff}}$ against a chosen threshold energy of 5 eV.[48] The molecule is said to be stable when $E_{\text{eff}}$ is below 5 eV, and

**TABLE 2: Yield of Ejected Hydrocarbon Species[a]**

| ejected species by groups | ejected fragments | total yield in 2100 trajectories | % of stable fragments | approx net intensity | % of fragments from top portion of chain |
|---|---|---|---|---|---|
| $C_nH_{2n+1}$ | $C_5H_{11}$ | 345 | 28 | 97 | 100 |
| | $C_4H_9$ | 97 | 43 | 40 | 100 |
| | $C_3H_7$ | 211 | 47 | 99 | 99 |
| | $C_2H_5$ | 175 | 70 | 123 | 96 |
| | $CH_3$ | 197 | 88 | 173 | 84 |
| $C_2H_{2n}$ | $C_5H_{10}$ | 87 | 2 | 2 | 100 |
| | $C_4H_8$ | 43 | 7 | 3 | 91 |
| | $C_3H_6$ | 122 | 13 | 16 | 83 |
| | $C_2H_4$ | 199 | 53 | 105 | 48 |
| $C_nH_{2n-2}$ | $C_2H_2$ | 207 | 68 | 141 | 28 |
| $C_nH_{2n-1}$ | $C_5H_9$ | 21 | 5 | 1 | 100 |
| | $C_4H_7$ | 13 | 8 | 1 | 85 |
| | $C_3H_5$ | 31 | 16 | 5 | 55 |
| | $C_2H_3$ | 45 | 78 | 35 | 33 |
| | H | 4429 | | | |
| | $H_2$ | 1205 | 100 | | |
| | M | 539 | 47 | | |

[a] Percentage of stable ejected species and the percentage of hydrocarbon fragments arising from the top portion of chain are given.

unstable when $E_{\text{eff}}$ is greater than the threshold. The choice of 5 eV is approximately that of a C−H bond (4.393 eV [69]) and is probably slightly larger than the lowest fragmentation channel but is a compromise choice so as not to throw out too many particles from the analysis.

The low-mass region of the calculated mass spectra consists of a number of hydrocarbon fragments. Some of these fragments correlate qualitatively well with the experiment.[27−33] There are some, however, which are barely detected in the simulation, but are in greater abundance in the experiment, and *vice versa*. The three major groups of hydrocarbon fragments which we will focus on are the $C_nH_{2n+1}$, $C_nH_{2n}$, and $C_nH_{2n-1}$ species. Besides, both atomic and molecular species are also found in this region of the spectra. They include atomic H, C, and S atoms as well as $H_2$ and the parent molecules, respectively. In the region between 190 and 840 amu, the calculated spectra also show peaks for single Au atoms, fragments of AuS and, and a variety of gold−thiolate clusters, $Au_xM_y$, where M is the alkanethiolate molecule in both studies.

**(i) $C_nH_{2n+1}$ Fragments.** The simulation predicts significant peaks of $C_nH_{2n+1}$ fragments for values of $n$ from 1 to 5. A correction for the stability of the ejected species (Table 2), however, adjusts this prediction; namely, whereas almost 90% of the $CH_3$ species are predicted to be stable and reach the detector, less than 30% of the $C_5H_{11}$ species will survive. The net effect of this correction is that the $CH_3$ species will be the most probable with a declining intensity to $C_4H_9$. There is an increase at $C_5H_{11}$ that will be discussed below.

The experimental data also exhibit significant intensities of $C_nH_{2n+1}^+$ ions, as shown in Figure 4a. On the basis of this agreement between the experimental data and the calculations, we thus propose that a plausible route for the formation of the $C_nH_{2n+1}^+$ ions in the mass spectra is due to direct fragmentation during the collision cascade.

The majority of the short $C_nH_{2n+1}$ fragments are found to originate from the top portion of the alkanethiolate chain as shown in Table 2. A similar observation was made by Taylor et al.[17,20] for a $C_5H_{11}$ overlayer adsorbed on a Pt surface. This prediction of the calculation has been experimentally verified in recent experiments of Langmuir−Blodgett films in which films with either orientation of the phospholipid chain phosphatidylcholine dipalmitoyl (DPPC) show preferred ejection of fragment ions from portions of the molecules closest to the surface, whether the phosphatidyl headgroup or the hydrocarbon tail group.[70]

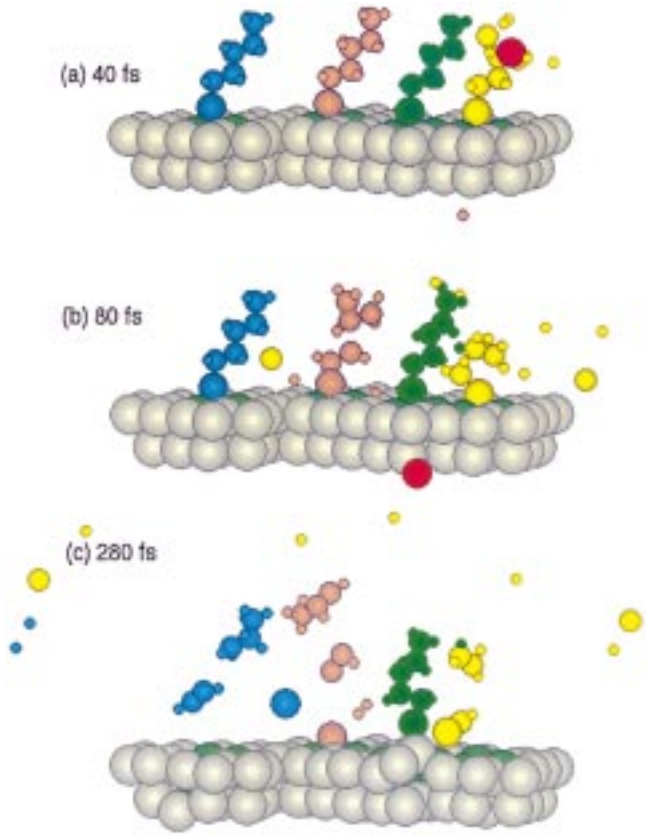


**Figure 5.** Sequence of collisional events leading to the ejection of $C_2H_4$, $C_3H_6$, and $C_3H_7$ fragments. The red Ar atom first collides with the yellow chain, initiating a series of collisions to produce a yellow $C_2H_4$ (one of the hydrogens comes from the adjacent green chain), an orange $C_3H_6$, and a blue $C_3H_7$ fragment. (See text for description of the events.)

The $C_nH_{2n+1}$ species are formed primarily due to direct collisions with fast-moving particles at the surface. Very often, the colliding particle is a species fragmented from the alkanethiolate chain, which in turn is produced by direct collisions of the incoming Ar atom with another alkanethiolate chain. On the other hand, the primary collision does not usually lead to the $C_nH_{2n+1}$ formation as it involves a collision with a more energetic Ar atom. Direct collisions with the Ar atom are more likely to knock off H atoms from the species resulting in, for example, a $C_nH_{2n}$ fragment that is discussed below. Figure 5 exemplifies both fragmentation of a chain by the Ar atom and subsequent formation of a $C_3H_7$ fragment. The red Ar atom first hits the yellow chain and knocks out a C atom (Figure 5a). This C atom then moves laterally across the surface to induce further collision with the blue alkanethiolate chain on the surface (Figure 5b) and ejects a $C_3H_7$ species from the top portion of the chain (Figure 5c).

In contrast to the experimental results, our simulations obtain a relatively high peak for the $C_5H_{11}$ fragment. Its formation involves the collision at the S−C1 bond of the chain due to the surface Au atom, and the cleavage of the bond to result in a $C_5H_{11}$ fragment and a S atom. This mechanism occurs quite frequently and the Au atom participating in the collision may originate from as much as 6 Å from the chain. The effective energy calculations do predict that the majority of the $C_5H_{11}$ fragments are unstable (Table 2); however, there is still

considerable intensity. It is unclear at this point why the calculations predict a relatively high intensity for the $C_5H_{11}$ fragment while these species are not observed in significant intensity in the experimental data. One possible reason may be due to the fact that the energy of the S−C bond is 2.6 eV compared to ∼4 eV for the C−C bond. The S−C bond is therefore more likely to fracture than the C−C bond of the alkanethiolate chain, thus giving rise to $C_5H_{11}$ fragments.

**(ii) $C_nH_{2n}$ Fragments and $C_2H_2$.** The $C_nH_{2n}$ fragments are formed during the collision cascade with almost the same probability as the $C_nH_{2n+1}$ fragments. The effective energy calculations summarized in Table 2, however, predict that almost all of the $C_nH_{2n}$ fragments will dissociate before reaching the detector with the exception of ethylene, $C_2H_4$, and acetylene, $C_2H_2$. Experimentally the ions of $C_2H_4$ and $C_2H_2$ are not observed in high yield in SIMS spectra of hydrocarbon films. The reason that the $C_2H_4$ and $C_2H_2$ fragments exist only as small peaks in the experiment is probably because of their low ionization probability. In fact, SIMS experiments of polymer films using post-ionization of neutral molecules show relatively high peaks for $C_2H_4^+$ and $C_2H_2^+$ ions in the mass spectrum.[27] The agreement between experiment and the calculation allows one to propose that the stable molecules of ethylene and acetylene are produced in the bombardment process. They will only be detected in abundance, however, in experiments in which neutral molecules can be observed.

In contrast to the $C_2H_{2n+1}$ fragments which predominantly arise from the top portion of the chain, there is not as strong a correlation with chain position for $C_2H_4$ and $C_2H_2$. Figure 5 shows one of the ways in which a $C_2H_4$ molecule can be formed from the bottom part of the chain. The red Ar atom first hits the yellow chain toward the top part of the hydrocarbon backbone (Figure 5a). The collision is so severe that the chain eventually breaks into various fragments including a $C_2H_3$ species and atomic carbon and hydrogen (Figure 5b). This $C_2H_3$ species is from the bottom portion of the chain and abstracts a H atom from the neighboring green chain to form into a $C_2H_4$ molecule (Figure 5, b and c). Abstraction reactions between fragments and molecules have been reported in earlier simulations of ethylidyne films on a metal surface.[16,17,19]

Figure 5 also shows the formation of a $C_3H_6$ species by direct collision of a laterally moving C atom fragmented from the yellow chain with the orange chain (Figure 5b). In general, these mechanisms suggest that hydrocarbon fragments are produced from direct collisions of the alkanethiolate chains with other fast-moving particles. Depending upon the point of contact in a collision, the chain may break into several fractions with different proportions of carbon and hydrogen atoms.

**(iii) $C_nH_{2n-1}$ Fragments.** The simulation predicts very low yields for the $C_nH_{2n-1}$ fragments even before making any correction for stability as given in Table 2. On the other hand, the experimental spectra consistently have comparable intensities of $C_nH_{2n-1}^+$ and $C_nH_{2n+1}^+$ as shown in Figure 4a. One plausible explanation for the discrepancy between the experimental observation and the prediction of the simulation is that the $C_nH_{2n-1}^+$ is produced via unimolecular decomposition of $C_nH_{2n+1}^+$ according to the reaction below,

$$C_nH_{2n+1}^+ \rightarrow C_nH_{2n-1}^+ + H_2 \qquad (6)$$

In other words, most of the $C_nH_{2n-1}^+$ fragments arise during the flight to the detector. This suggestion appears to be supported by the evidence that the majority of the larger $C_nH_{2n-1}$ fragments formed during the collision cascade are unstable (Table 2).

**(iv) Other Hydrocarbon Species.** The simulation also predicts a variety of other hydrocarbon species. There are fragments such as CH, $CH_2$, and $C_2H$ species. The $CH^-$ and $CH_2^-$ peaks are observed (Figure 4b) with higher intensity in the negative SIMS spectrum than their corresponding cations (Figure 4a) in the positive spectrum. The $C_2H^-$ species is only detected in the negative spectrum. Again, these fragments are likely to be formed as a result of direct collisions along the hydrocarbon portion of the chain and the mechanism is similar to that already described.

**(v) H, $H_2$, C, and S Species.** The most intense peaks obtained in the simulation are H atom and $H_2$ molecule. The high yield of H atoms is due to their relatively exposed positions which make them vulnerable to being ejected by direct collisions. Molecular $H_2$, on the other hand, must involve some reaction. The simulations predict that in ∼80% of these molecules the H atoms came from different chains. As reported earlier, H abstraction reactions are relatively common during the collision cascade.[19]

Experimentally, the peaks $H^+$, $H_2^+$, $H_3^+$, $H^-$, and $H_2^-$ are observed in the SIMS spectra for a plethora of organic films. In some respects this is surprising given the high ionization energies and small electron affinities. For example, the ionization energy of H atom is 13.6 eV and that of $H_2$ is 15.4 eV[71] and the electron affinities are 0.75 and −0.72 eV.[72] One plausible explanation for the large occurrence of $H^+$ and $H^-$ is that they are formed by relatively hard collisions during the collision cascade. Thus, at least part of the ionization energy comes from the collision process. It is interesting to speculate on the formation of $H_2^+$ and $H_2^-$. Could they be formed from $H^+$ and $H^-$ ions knocked off in the collision cascade which abstract a H atom from another molecule? This could explain a large population of a species that has a relatively large ionization energy or small electron affinity. Moreover, could this general process also participate significantly in the formation of the protonated and deprotonated molecular ions that are often observed in SIMS spectra?

The second most intense monatomic peak in the simulation corresponds to the C atom. It is normally recorded as a $C^-$ peak in the negative spectrum, although a very small $C^+$ peak is also observed in the positive spectrum. As shown in Figure 5 it is facile for a C atom to be released from a hydrocarbon chain (yellow chain) upon direct collision with other particles. Depending on the site of collision, the C atom may arise from the top or bottom parts of the chain.

Peaks for the sulfur moieties $S^-$ and $SH^-$ are always observed in the experimental spectrum. While the atomic S peak is also recorded in the simulation, we have only obtained an extremely low yield for the SH species. This is not surprising since the S−H potential employed in the calculations is designed for long-range van der Waals interactions rather than bonding interactions and thus is relatively weak. The mechanism of formation of a S atom involves the collision of a rising surface Au atom with an alkanethiolate chain at the S−C1 site thereby causing a scission at the bond. The process usually leads to the displacement of the S atom from the original 3-fold site. The S atom may then eject as a single S atom, remain on the surface, and move laterally across the surface to induce further collisions or bond with neighboring atoms or molecules and eject as a combined unit. In the latter case, it may lead to the formation of clusters such as AuS or AuSM which have also been observed experimentally.

**(vi) Parent Molecule.** The ejection of intact parent thiolate molecules, M, appears to be a highly probable process in the

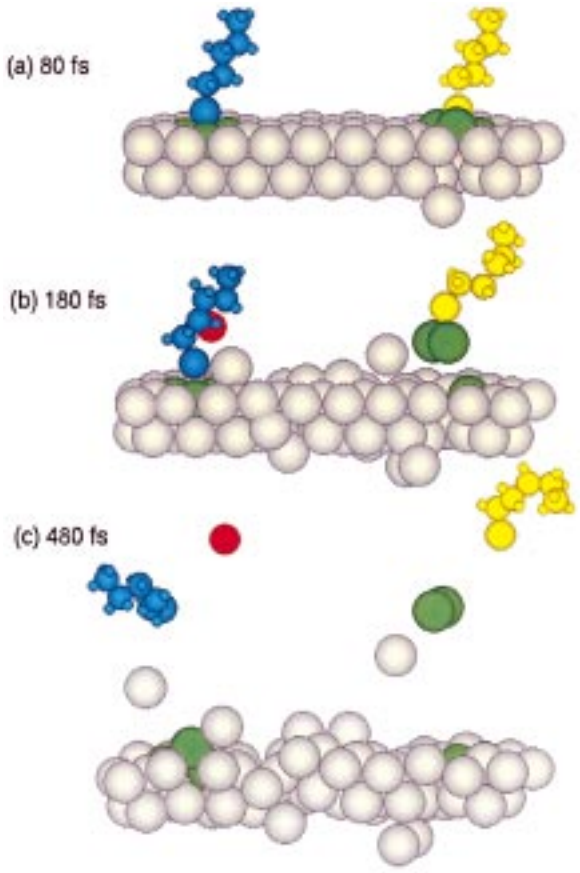


**Figure 6.** Two mechanisms for the ejection of intact alkanethiolate molecules. The yellow chain is lifted by its 3-fold Au atoms (green) and the blue chain by a rising Au atom from the surface. In both cases, the collisions occur through the S site of the chains. The red sphere is the Ar atom. (See text for description of the events.)

simulation even after an attempt to correct for stability as shown in Table 2. In contrast to the effective energy calculations for the small hydrocarbon species, in this case the potential is certainly deficient. The CH potential considers the molecule stable as all C atoms have four neighbors. Since the S potential is not many-body in nature, it does not recognize that the S atom is undercoordinated.

Experimentally, the thiolate species is observed in low yield as a negative ion from gold surfaces but in much larger relative yields if a Ag substrate is used.[27−29,33] This indicates that the thiolate molecule can in fact be ionized and is stable enough to be detected. The difference between the Ag and Au substrates is that the Ag−S adsorption energy is weaker than the Au−S adsorption energy.[28,29] In most cases in which the entire alkanethiolate chain is able to eject intact, it is hit by a Au atom at the surface. Figure 6 shows the ejection of alkanethiolate chains through collisions with Au atoms on the surface. As the Ar atom bombards the Au surface, the input energy causes two of the 3-fold Au atoms (green) to push up on the yellow chain (Figure 6, b and c). Other Au atoms may also induce the ejection by hitting at the S site of a chain. The ejection is usually coupled with the weakening of the 3-fold bond as a result of the displacement of the 3-fold Au atoms. This is illustrated by the blue chain in Figure 6. A surface Au atom collides with the blue chain at the S site thus lifting up the entire chain. As we will see later, the ejection of this parent molecule is important to the formation of gold−thiolate clusters.

**(vii) Gold−Thiolate ($Au_xM_y$) Clusters.** The formation of the gold−thiolate clusters appear to be sensitive to the chemical environment.[28,29,34,37] Factors such as geometrical positions and concerted motions of the constituent species in a cluster have been identified to be essential to their formation, as in the case of $AuM_2$ in our previous study.[38,39] Here, we will investigate the other $Au_xM_y$ clusters to see if there exists a general pattern for alkanethiolate molecules and Au atoms to come together and form into a particular gold−thiolate cluster. Information such as the relative positions between Au atoms and alkanethiolate molecules that give rise to $Au_xM_y$ clusters will also be addressed.

The AuM species are the most abundant molecules among the gold−thiolate clusters recorded in the calculated spectrum, Table 3. Very often, they are found to be the precursor for the formation of gold−thiolate clusters with multiple Au atoms or alkanethiolate molecules. This occurs through the combination of a Au atom with a nearby alkanethiolate molecule to form a AuM species before subsequent attachment of other neighboring (although not necessarily nearest neighbor) Au atoms or alkanethiolate molecules.

While Au atoms of close neighbors may exist as dimers prior to combination with thiolate molecules, it is not commonly observed for alkanethiolates to first aggregate into dialkanethiolates. It follows that the use of modified S−S potential does not seem to play an important role in the formation of gold−thiolate clusters. This may be due to the fact that alkanethiolate molecules are usually lifted by the underlying Au atoms and they are mobilized as a result of collisions generated across the Au substrate after the Ar impact. In situations where the momentum of the Au and thiolate species are directed toward one another and providing that they are in close proximity, it is likely that their concerted motions may facilitate the combination process to form gold−thiolate clusters. Figure 7 illustrates the formation of a $Au_2M$ and a $AuM_2$ molecule. The two surface Au atoms (pink) rise due to Ar collision (Figure 7a). One of the pink Au atoms moves toward the blue chain and the other to the orange chain. At the same time, a 3-fold Au atom (green) of the yellow chain is also lifted and pushes toward the blue chain to form into a AuM molecule (Figure 7b). As the first pink Au atom and the AuM molecule leave the surface, they combine to form a $Au_2M$ species, Figure 7c. Following the displacement of the green Au atom, the 3-fold structure for the yellow chain is weakened. Subsequently, the chain is attracted to the second pink Au atom. At the same time, the orange chain is also mobilized and the concerted motions of these three entities result in the formation of a $AuM_2$ molecule.

The Au atoms involved in the gold -thiolate clusters are often found to be one of the 3-fold Au atoms attached to the alkanethiolate chain. Depending upon the direction of momentum of these Au atoms, they may move toward or away from their attached alkanethiolate chain. In the former case, the 3-fold Au atoms and the chain signify an already-combined route to the gold−thiolate formation. When these Au atoms move away from the chain, however, the formation will depend on the reactions with other neighboring chains to form into clusters.

Table 3 shows the statistics of the original distances between Au atoms and alkanethiolate molecules prior to the Ar impact, which lead to the formation of various gold−thiolate clusters. In general, the majority of Au atoms in gold−thiolate clusters were originally close neighbors less than 6 Å from the alkanethiolate molecules. These Au atoms contribute 60%−90% of the total Au atoms involved in the clusters, of which 10%−30% are those Au atoms which occupy one of the 3-fold sites adjacent to the alkanethiolate molecule whose bond distances was less than 3 Å. It is also possible for Au atoms which are

**TABLE 3: Total Yield of Ejected Gold−Thiolate Clusters**[a]

| molecules | total yield in 2100 trajectories | Au−S distances[b] (%) | distances <6 Å for Au−S (%) | distances >6 Å for Au−S (%) | distances <5 Å for M−M (%) | distances <3 Å for nearest Au−Au neighbors (%) | first layer Au atoms (%) |
|---|---|---|---|---|---|---|---|
| Au | 411 | | | | | | 94 |
| AuM | 217 | 17 | 70 | 30 | | | 95 |
| $AuM_2$ | 90 | 13 | 69 | 31 | 99 | | 99 |
| $AuM_3$ | 13 | 13 | 62 | 39 | 92 | | 100 |
| $Au_2M_2$ | 22 | 24 | 68 | 32 | 100 | 68 | 96 |
| $Au_2M_3$ | 10 | 15 | 67 | 33 | 90 | 40 | 90 |
| $Au_2M$ | 23 | 30 | 89 | 11 | | 74 | 100 |
| AuS | 20 | 15 | 55 | 45 | | | 100 |
| AuSM | 8 | 0 | 56 | 44 | 88 | | 100 |

[a] The distances between Au atoms and alkanethiolate molecules measured at the S site, and where the Au atoms arise to form into clusters are also listed. The figures for Au−S distances less than 6 Å also include those less than 3 Å between the threefold Au atoms and thiolate molecules. [b] Less than 3 Å with the Au atom in threefold sites.

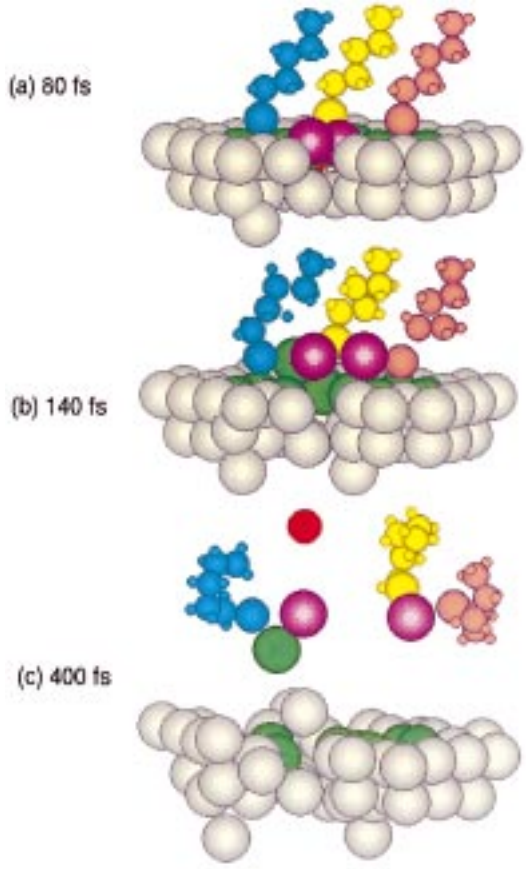


**Figure 7.** Combination of Au atoms with alkanethiolate chains to give a $Au_2M$ and a $AuM_2$ molecule. The $Au_2M$ species consists of a blue chain with one green and one pink Au atoms. The $AuM_2$ species consists of one yellow and one orange chains with a pink Au atom. (See text for description of the events.)

more than 6 Å from a thiolate chain to participate in a cluster with that chain. In fact, 10%−45% of the Au atoms involved in gold−thiolate clusters originate more than 6 Å from the thiolate chain. These Au atoms are commonly seen to move laterally across the surface to combine with the alkanethiolates.

In the case of clusters involving Au dimers (e.g. $Au_2M$ and $Au_2M_2$) over 65% of the two Au atoms arise from nearest neighbors less than 3 Å from one another. They are usually pushed up concurrently by the bulk atoms two or three layers below. Most of the clusters formed involving more than one alkanethiolate chain originate from nearest neighbors with a separation of about 5 Å. Although the chains are close to one another, our potential parameters are chosen such that they are not bonded initially and have no direct interaction between them. In fact, the chains are lifted via the mechanisms described earlier and can be captured by nearby Au atoms to form into gold-thiolate clusters.

**(viii) Au, AuSM Species and Gold-Fragment Species.** The high peak intensity for atomic Au atoms arise from the Ar-induced collision cascade in the solid. Although it is likely that the Au atoms will collide with the alkanethiolates, some Au atoms are ejected as atomic species. Table 3 shows that over 90% of the ejected Au atoms arise from first layer of the substrate. There are virtually no Au dimers found in our study although they are detected in high yield experimentally. Undoubtedly the lack of Au dimers is because the enhanced Au−S interaction pulls Au dimers into gold-thiolate species.

We turn next to the AuS and AuSM species observed in the simulation. These moieties are recorded as $AuS^-$ and $AuSMH^-$ peaks in the negative SIMS spectra. Table 3 shows that all the Au atoms involved in these two species arise from the first layer of the Au substrate. Moreover, about 55% of them are formed between close neighbors of alkanethiolate chains and Au atoms originating within distances less than 6 Å.

The formation of a AuS species first requires a single S atom at the surface. This can be achieved by having a Au atom collide with an alkanethiolate chain at the S−C1 bond thereby giving a free S atom and a $C_5H_{11}$ fragment. The S atom then combines with that Au atom to form into a AuS molecule. In some cases, the AuS species may further combine with another alkanethiolate to produce a AuSM molecule. Conversely, the Au atom may bond with an alkanethiolate chain before picking up a S atom. In either case, the three entities are close to one another and the combination process is facilitated by their concerted motions.

Experimentally, as seen in Figure 4a, there are significant intensity peaks corresponding to $AuCH_2^+$ and $Au(CH_2)_2^+$. These peaks are not observed in the simulation because we have assumed a weak van der Waals interaction between Au and C atoms (Table 1). To do a better job at describing the various moieties with gold and part or all of the thiolate chain, a true many-body potential similar to the Brenner potential for hydrocarbons is needed. Development of such a potential, however, is not a trivial task.

**(ix) Other Ejected Species.** A number of low-yield peaks are found along the base of the calculated spectra. Such species include a variety of sulfur atoms bonded to hydrocarbon fragments of different chain lengths (e.g. $SCH_2$, $SC_2H_3$, $SC_3H_6$) and Au atoms bonded to the fragmented alkanethiolate chains (e.g. $AuSCH_2$, $AuS(CH_2)_3$, $AuSC_5H_5$, $Au_2S_2C_{10}H_{21}$). Other large gold−thiolate clusters are also recorded which include the $AuM_3$, $Au_2M_3$, and $Au_3M_2$ species. Some of these fragments and clusters such as the $AuSCH_2$, $AuS(CH_2)_3$, $Au_2M_3$, and $Au_3M_2$ species are also seen in the experiment. Due to their

extremely low ejection rate in the simulation, these species are not analyzed in detail here.

## Conclusions

Molecular dynamics simulations have been performed using many-body interaction potentials to describe energetic particle bombardment of an alkanethiolate film on Au(111). We have emphasized the nature and intensity of the various ejected species and have made direct comparisons to experimental data. For the hydrocarbon fragments we have estimated the effect of unimolecular decomposition during the flight time to the detector. To reasonably estimate the gold−thiolate clusters we developed a Au−S interaction potential in which the bond strength varies with height of the Au and S species above the surface.

Peaks for $C_nH_{2n+1}$ fragments are of significant intensity in both the simulation and experimental studies that detect positive ions. In addition, the intensity decreases as $n$ increases in both the experimental and calculated spectra. The majority of $C_nH_{2n}$ fragments (for $n \geq 3$) recorded in the simulation are unstable and predicted to decompose into smaller species at a later time. Only the $C_2H_4$ and $C_2H_2$ species remain as relatively high-intensity peaks in the simulation. Although these peaks are observed as cations in experimental studies on polymers, in general they are not observed. We believe that they would be observed in higher intensity in experiments using postionization in which neutral molecules can be detected. In contrast with experimental observations, the simulations suggest very little intensity for $C_nH_{2n-1}$ fragments. We propose that they form according to the unimolecular decomposition reaction,

$$C_nH_{2n+1}^{+} \rightarrow C_nH_{2n-1}^{+} + H_2$$

The gold−thiolate clusters identified in the simulation are AuM, $AuM_2$, $Au_2M$, $Au_2M_2$, AuS, and AuSM. The model then suggests that the important step in the formation of a sputtered $Au_xM_y$ molecule is the release of intact alkanethiolate molecules from the surface. This is achieved by a less energetic Au atom colliding the chain at the S site thereby lifting the entire molecule up. Once the chain is slightly above the surface, it can be captured by Au atoms to form into gold−thiolate clusters. In many cases, AuM molecules are formed before further attachment of other Au atoms or alkanethiolate molecules. On the other hand, where Au dimers are involved the participating Au atoms are frequently part of a pair prior to bonding with other species. The model provides a basis for expecting that the relative yields of the various gold−thiolate clusters should reflect the structure and the local environment of the SAM surface.

The rather close correlation between the experimental spectra and the "mass spectra" predicted by the model provides confidence that the emission mechanisms underlying the model may not be far from those operating in practice. This is a very encouraging further step to providing a theoretical mechanistic underpinning of the experimental observation that static SIMS is indeed a surface-sensitive technique which is suitable for probing the chemistry of complex organic surfaces.

**Acknowledgment.** The authors would like to acknowledge the support of UMIST for the provision of a Chemistry Department Research Studentship and an Overseas Research Studentship for K.S.S.L. The support of the National Science Foundation through the Chemistry Division the CRIF program and the MRI program are gratefully acknowledged by B.J.G. Additional computational resources were provided in part by the IBM Selected University Resource Program and the Center for Academic Computing at Penn State. Support from the UK Engineering and Physical Sciences Research Council is also gratefully acknowledged by J.C.V.

## References and Notes

(1) *The Proceedings of the Eleventh International Conference on SIMS, SIMS XI*; Gillen, G., Lareau, R., Bennett, J., Stevie, F., Eds.; John Wiley & Sons Ltd.: New York, 1998.
(2) Harrison, D. E., Jr.; Levy, N. S.; Johnson, J. P.; Effron, H. M. *J. Appl. Phys.* **1968**, *39*, 3742.
(3) Harrison, D. E., Jr.; Moore, W. L., Jr.; Holcombe, H. T. *Radiat. Eff.* **1973**, *17*, 167.
(4) Harrison, D. E., Jr.; Delaplain, C. B. *J. Appl. Phys.* **1976**, *47*, 2252.
(5) Garrison, B. J.; Winograd, N.; Harrison, D. E., Jr. *J. Chem. Phys.* **1978**, *69*, 1440.
(6) Foley, K. E.; Garrison, B. J. *J. Chem. Phys.* **1980**, *72*, 1018.
(7) Garrison, B. J.; Wucher, A. *Surf. Sci.* **1992**, *260*, 257.
(8) Rosencrance, S. W.; Burnham, J. S.; Sanders, D. E.; He, C.; Garrison, B. J.; Winograd, N. *Phys. Rev. B* **1995**, *52*, 6006.
(9) Shapiro, M. H.; Tombrello, T. A. *Nucl. Instrum. Methods B* **1994**, *84*, 453.
(10) Betz, G.; Husinsky, W. *Nucl. Instrum. Methods B* **1995**, *102*, 281.
(11) Shapiro, M. H.; Tombrello, T. A. *Nucl. Instrum. Methods B* **1991**, *62*, 35.
(12) Broomfield, K.; Stansfield, R. A.; Clary, D. C. *Surf. Sci.* **1990**, *227*, 369.
(13) Garrison, B. J. *J. Am. Chem. Soc.* **1980**, *102*, 6553.
(14) Garrison, B. J. *J. Am. Chem. Soc.* **1982**, *104*, 6211.
(15) Lauderback, L. L.; Ang. M. L.; Murray, H. C. *J. Chem. Phys.* **1990**, *93*, 6041.
(16) Taylor, R. S.; Garrison, B. J. *Langmuir* **1995**, *11*, 1220.
(17) Taylor, R. S.; Garrison, B. J. *Int. J. Mass. Spectrom. Ion Processes* **1995**, *143*, 255.
(18) Taylor, R. S.; Garrison, B. J. *Chem. Phys. Lett.* **1994**, *230*, 495.
(19) Taylor, R. S.; Garrison, B. J. *J. Am. Chem. Soc.* **1994**, *116*, 4465.
(20) Taylor, R. S.; Brummel, C. L.; Winograd, N.; Garrison, B. J.; Vickerman, J. C. *Chem. Phys. Lett.* **1995**, *233*, 575.
(21) Nuzzo, R. G.; Allara, D. L. *J. Am. Chem. Soc.* **1983**, *105*, 4481.
(22) Chidsey, C. E. D.; Bertozzi, C. R.; Putvinski, T. M.; Mujsce, A. M. *J. Am. Chem. Soc*. **1990**, *112*, 4301.
(23) Ulman, A.; Evans, S. D.; Shnidman, Y.; Eilers, R.; Chang, J. C. *J. Am. Chem. Soc.* **1991**, *113*, 1499.
(24) Pale-Grosdemange, C.; Simon, E. S.; Prime, K. L.; Whitesides, G. M. *J. Am. Chem. Soc*. **1991**, *113*, 12.
(25) Bain, C. D.; Whitesides, G. M. *Langmuir* **1989**, *5*, 1370.
(26) Vickerman, J. C.; Brown, A. C.; Reed, M. *Secondary Ion Mass Spectrometry*; Clarendon Press: Oxford, UK, 1989.
(27) Vickerman, J. C.; Briggs, D.; Henderson, A. *The Static SIMS Library*; Surface Spectra Ltd.: Manchester, UK, 1997.
(28) Canry, J. C. Ph.D. Thesis, UMIST, 1998.
(29) Canry, J. C.; Vickerman, J. C. In *The Proceedings of the Tenth International Conference on SIMS, SIMS X*; Benninghoven, A., Hagenhoff, B., Werner, H. W., Eds.; John Wiley & Sons Ltd.: New York, 1997; p 623.
(30) Tarlov, M. J.; Newman, J. G. *Langmuir* **1992**, *8*, 1398.
(31) Hagenhoff, B.; Benninghoven, A.; Spinke, J.; Liley, M.; Knoll, W. *Langmuir* **1993**, *9*, 1622.
(32) Leggett, G. J.; Davies, M. C.; Jackson, D. E.; Tendler, S. J. B. *J. Chem. Soc., Faraday Trans.* **1993**, *89*, 179.
(33) Rading, D. Ph.D. Thesis, Münster, 1997.
(34) Canry, J.-C.; Vickerman, J. C. In *ECASIA*; Mathieu, J. H., Reihl, B., Briggs, D., Eds.; John Wiley & Sons: New York, 1995; p 903.
(35) Offord, D. A.; John, C. M.; Linford, R. M.; Griffin, J. H. *Langmuir* **1994**, *10*, 883.
(36) Offord, D. A.; John, C. M.; Griffin, J. H. *Langmuir* **1994**, *10*, 761.
(37) Wood, M. Ph.D. Thesis, The Penn State University, 1995.
(38) Liu, K. S. S.; Vickerman, J. C.; Garrison, B. J. *Radiat. Eff. Defects Solids* **1997**, *142*, 205.
(39) Liu, K. S. S.; Vickerman, J. C.; Garrison, B. J. In *The Proceedings of the Eleventh International Conference on SIMS, SIMS XI*; Gillen, G., Lareau, R., Bennett, J., Stevie, F., Eds.; John Wiley & Sons Ltd.: New York, 1998; p 443.
(40) Winograd, N.; Garrison, B. J. In *Ion Spectroscopies for Surface Analysis*; Czanderna, A. W., Hercules, D. M., Eds.; Plenum Press: New York, 1991; p 45.
(41) Garrison, B. J. *J. Chem. Soc. Rev.* **1992**, *21*, 155.
(42) Bernardo, D. N.; Bhatia, R.; Garrison, B. J. *Comput. Phys. Commun.* **1994**, *80*, 259.
(43) Harrison, D. E., Jr. *CRC Crit. Rev. Solid State Matter Sci.* **1988**, *14*, S1.

(44) The correction to the screening factor in the Molière eq 6 of: O'Connor, D. J.; MacDonald, R. J. *Radiat. Eff.* **1977**, *34*, 247.
(45) Stave, M. S.; Sanders, D. E.; Raeker, T. J.; DePristo, A. E. *J. Chem. Phys.* **1990**, *93*, 4413.
(46) Raeker, T. J.; DePristo, A. E. *Int. Rev. Phys. Chem.* **1991**, *10*, 1.
(47) Kelchner, C. L.; Halstead, D. M.; Perkins, L. S.; Wallace, N. M.; DePristo, A. E. *Surf. Sci.* **1994**, *310*, 425.
(48) Chatterjee, R.; Postawa, Z.; Winograd, N.; Garrison, B. J. *J. Phys. Chem.*, submitted for publication.
(49) Mahaffy, R.; Bhatia, R.; Garrison, B. J. *J. Phys. Chem. B* **1997**, *101*, 771.
(50) Bhatia, R.; Garrison, B. J. *Langmuir* **1997**, *13*, 765.
(51) Bhatia, R.; Garrison, B. J. *Langmuir* **1997**, *13*, 4038.
(52) Brenner, D. W. *Phys. Rev. B* **1990**, *42*, 9458.
(53) Brenner, D. W.; Harrison, J. A.; White, C. T.; Colton, R. J. *Thin Solid Films* **1991**, *206*, 220.
(54) Garrison, B. J.; Kodali, P. B. S.; Srivastava, D. *Chem. Rev.* **1996**, *96*, 1327.
(55) Tupper, K. J.; Brenner, D. W. *Thin Solid Films* **1994**, *253*, 185.
(56) Tupper, K. J.; Brenner, D. W. *Langmuir* **1994**, *10*, 2335.
(57) Alfonso, D. R.; Ulloa, S. E.; Brenner, D. W. *Phy. Rev. B* **1994**, *49*, 4948.
(58) Brenner, D. W.; Harrison, J. A. *Technology* **1992**, *71*, 1821.
(59) Harrison, J. A.; White, C. T.; Colton, R. J.; Brenner, D. W. *Phy. Rev. B* **1992**, *46*, 9700.
(60) Harrison, J. A.; Brenner, D. W.; White, C. T.; Colton, R. J. *Thin Solid Films* **1991**, *206*, 213.
(61) Chatterjee, R.; Garrison, B. J. *Radiat. Eff. Defects Solids* **1997**, *142*, 127.
(62) Zaric, R.; Pearson, B.; Krantzman, K. D.; Garrison, B. J. In *The Proceedings of the Eleventh International Conference on SIMS, SIMS XI*; Gillen, G., Lareau, R., Bennett, J., Stevie, F., Eds.; John Wiley & Sons Ltd.: New York, 1998; p 601.
(63) Zaric, R.; Pearson, B.; Krantzman, K. D.; Garrison, B. J. *Int. J. Mass Spectrom. Ion Processes* **1998**, *174*, 155.
(64) Girifalco, L. A.; Weizer, V. G. *Phys. Rev.* **1959**, *114*, 687.
(65) Allen, M. P.; Tildesley, D. J. *Computer Simulation in Liquids*; Oxford University Press: Oxford, UK, 1987.
(66) Huber, K. P.; Herzberg, G. *Molecular spectra and molecular structure IV. Constants of diatomic molecules*; Van Nostrand Reinhold Co.: New York, 1979.
(67) Smith, R.; Harrison, D. E. Jr.; Garrison, B. J. *Phys. Rev. B* **1989**, *40*, 93.
(68) Wucher, A.; Garrison, B. J. *Phys. Rev. B* **1992**, *46*, 4855.
(69) Lewis, G. N.; Randall, M. *Thermodynamics*, 2nd ed.; McGraw−Hill: New York, 1961; p 682.
(70) Pacholski, M. L.; Cannon, D. M.; Ewing, A. G.; Winograd, N., to be published.
(71) *CRC Handbook of Chemistry and Physics*, 62nd ed.; Weast, R. C., ed.; CRC Press Inc.: Boca Raton, FL, 1981.
(72) Vedeneyev, V. I.; Gurvich, L. V.; Kondrat'yev, V. N.; Medvedev, V. A.; Frankevich, Ye. L. *Bond energies ionization potentials and electron affinities*; Edward Arnold (Publishers) Ltd.: London, 1966.